H I Deficiencies and Asymmetries in HIPASS Galaxies.

T.N. Reynolds[1,2]★, T. Westmeier[1,2], L. Staveley-Smith[1,2]
[1]*International Centre for Radio Astronomy Research (ICRAR), The University of Western Australia, 35 Stirling Hwy, Crawley, WA, 6009, Australia*
[2]*ARC Centre of Excellence for All Sky Astrophysics in 3 Dimensions (ASTRO 3D)*

Accepted 2020 October 06. Received 2020 September 29; in original form 2020 September 03

ABSTRACT
We present an analysis of the sky distribution of neutral hydrogen (H I) deficiency and spectral asymmetry for galaxies detected by the H I Parkes All-Sky Survey (HIPASS) as a function of projected environment density. Previous studies of galaxy H I deficiency using HIPASS were sensitive to galaxies that are extremely H I rich or poor. We use an updated binning statistic for measuring the global sky distribution of H I deficiency that is sensitive to the average deficiencies. Our analysis confirms the result from previous studies that galaxies residing in denser environments, such as Virgo, are on average more H I deficient than galaxies at lower densities. However, many other individual groups and clusters are not found to be on average significantly H I poor, in contradiction to previous work. In terms of H I spectral asymmetries, we do not recover any significant trend of increasing asymmetry with environment density as found for other galaxy samples. We also investigate the correlation between H I asymmetry and deficiency, but find no variation in the mean asymmetry of galaxies that are H I rich, normal or poor. This indicates that there is either no dependence of asymmetry on H I deficiency, or a galaxy's H I deficiency only has a small influence on the measured H I asymmetry that we are unable to observe using only integrated spectra.

Key words: galaxies: general – galaxies: groups: general – galaxies: clusters: general – radio lines: galaxies

1 INTRODUCTION

Galaxies are observed with morphologies spanning from active star forming, late-type systems through to passive, early-types. Across morphologies, asymmetries are observed in the stellar and gaseous (atomic hydrogen, H I) disks, and galaxies are found with gas contents ranging from gas-rich to gas-poor. A late-type, star forming galaxy in isolation and without any external influences is most likely to appear symmetrical as the morphology is primarily driven by the groups, rather than in isolated, field galaxies and galaxies in low density groups (e.g. Chamaraux et al. 1980; Solanes et al. 2001; Verdes-Montenegro et al. 2001; Boselli & Gavazzi 2009; Chung et al. 2009; Kilborn et al. 2009; Hess & Wilcots 2013).

There are many external (e.g. tidal and ram pressure stripping) and internal (e.g. star formation and supernova feedback) mechanisms proposed for causing the diversity of galaxy morphologies and giving rise to observed asymmetries, with the occurrence of

- Def HI может быть связан:
- A) с израсходованием газа на SF
- C) с supernovae feedback
- B) с ram pressure stripping
- C) с tidal stripping

Вопрос: как дефицит HI связан с плотностью окружения?

New H I scaling relations to probe the H I content of galaxies via global H I-deficiency maps

H. Dénes,[1,2★] V. A. Kilborn[1] and B. S. Koribalski[2]

[1]*Centre for Astrophysics & Supercomputing, Swinburne University of Technology, PO Box 218, Hawthorn, VIC 3122, Australia*
[2]*Australia Telescope National Facility, CSIRO Astronomy and Space Science, PO Box 76, Epping, NSW 1710, Australia*

Accepted 2014 June 30. Received 2014 June 27; in original form 2013 August 9

ABSTRACT

We present new multiwavelength scaling relations between the neutral hydrogen content (H I) and the stellar properties of nearby galaxies selected from the H I Parkes All-Sky Survey (HIPASS). We use these new scaling relations to investigate the environmental dependence of the H I content of galaxies. We find that galaxies in high-density environments tend to have on average less H I than galaxies with the same stellar mass in low-density environments. Our new H I scaling relations allow us to identify individual galaxies, as well as group/cluster environments, that have an 'anomalous' H I content. We map the global distribution of H I-deficient and H I-excess galaxies on the sky and compare it to the large-scale structure of galaxies. We find galaxy clusters to be H I deficient, and we identify that the regions surrounding clusters tend to be H I excess. Finally, we demonstrate the potential of using H I scaling relations to predict future H I surveys based on an optical redshift survey. We apply our scaling relations to 16 709 galaxies in the 6dF Galaxy Survey that lie in the HIPASS volume and compare our predictions to the measurements. We find that scaling relations are a good method to estimate the outcome of H I surveys.

Key words: surveys – galaxies: clusters: general – galaxies: evolution – galaxies: general – galaxies: groups: general – radio lines: galaxies.

Рассматриваются single galaxies для которых S/N >9 в линии HI

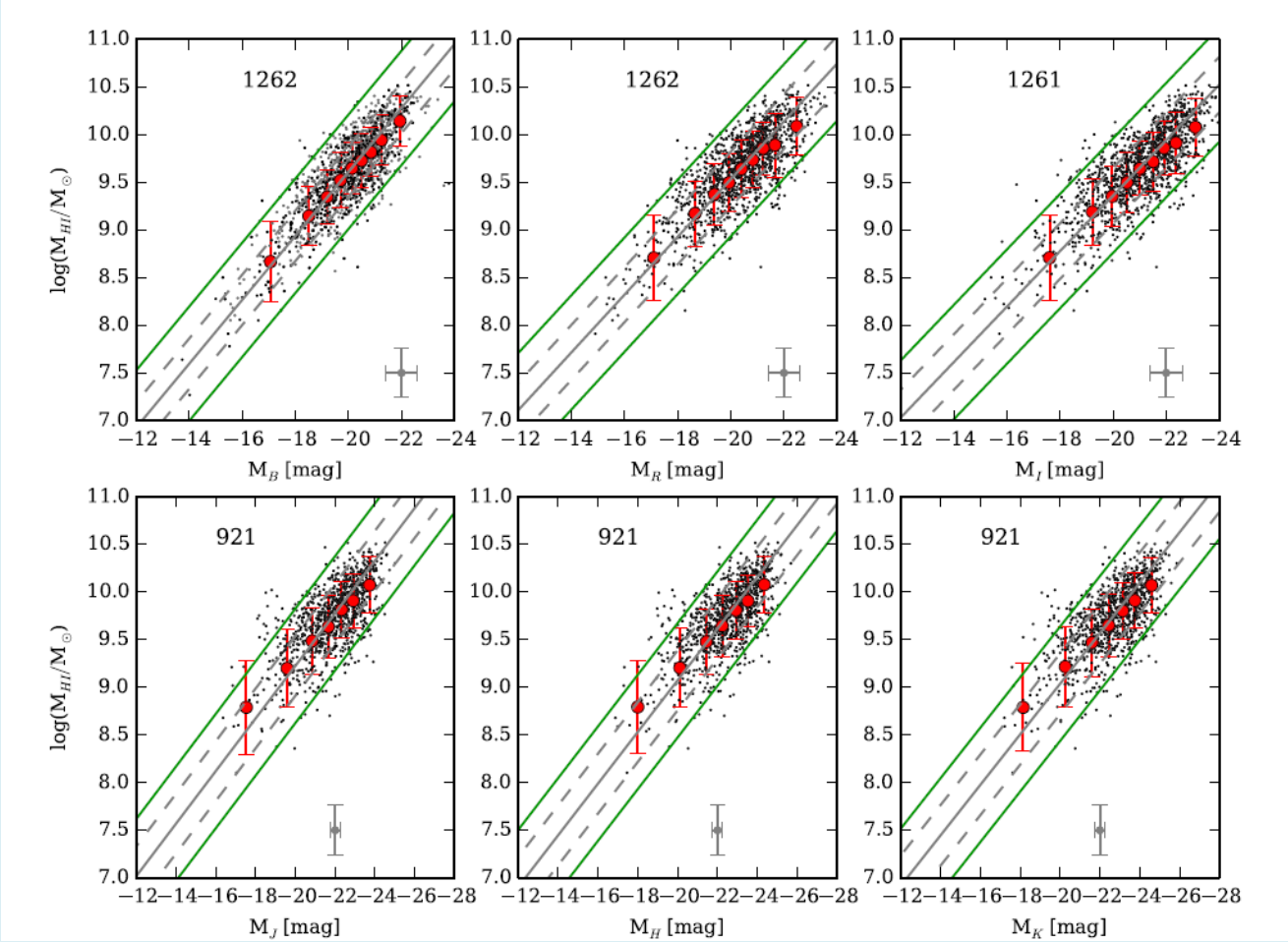

$$\mathrm{DEF_{H\,I}} = \log[M_{\mathrm{H\,I exp}}] - \log[M_{\mathrm{H\,I obs}}], \quad (1)$$

where $M_{\mathrm{H\,I exp}}$ is the expected H I mass, usually calculated from H I scaling relations, and $M_{\mathrm{H\,I obs}}$ is the calculated H I mass from the measurements.

Более 5000 галактик с Vr =300-6000 км/с

Критика предшественников; результаты чувствительны к наличию отскакивающих галактик. Пересматриваются данные HIPASS (15.5’). Другая обработка с учетом стат.веса.

Отслеживается

про

$$A_{\text{flux}} = \frac{I_1}{I_2} = \frac{\sum_{v_{\text{low}}}^{V_{\text{sys},w20}} I dv}{\sum_{V_{\text{sys},w20}}^{v_{\text{high}}} I dv},$$

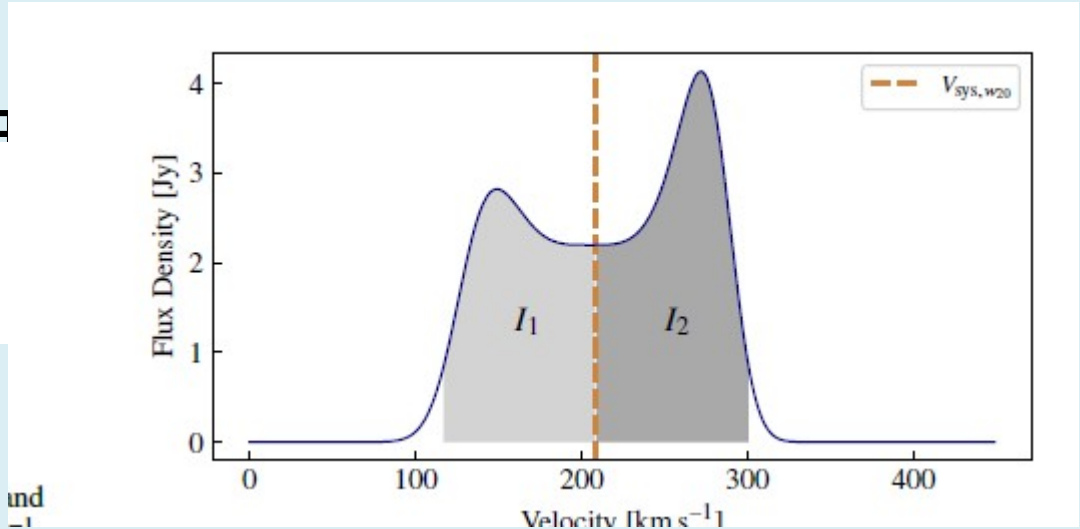

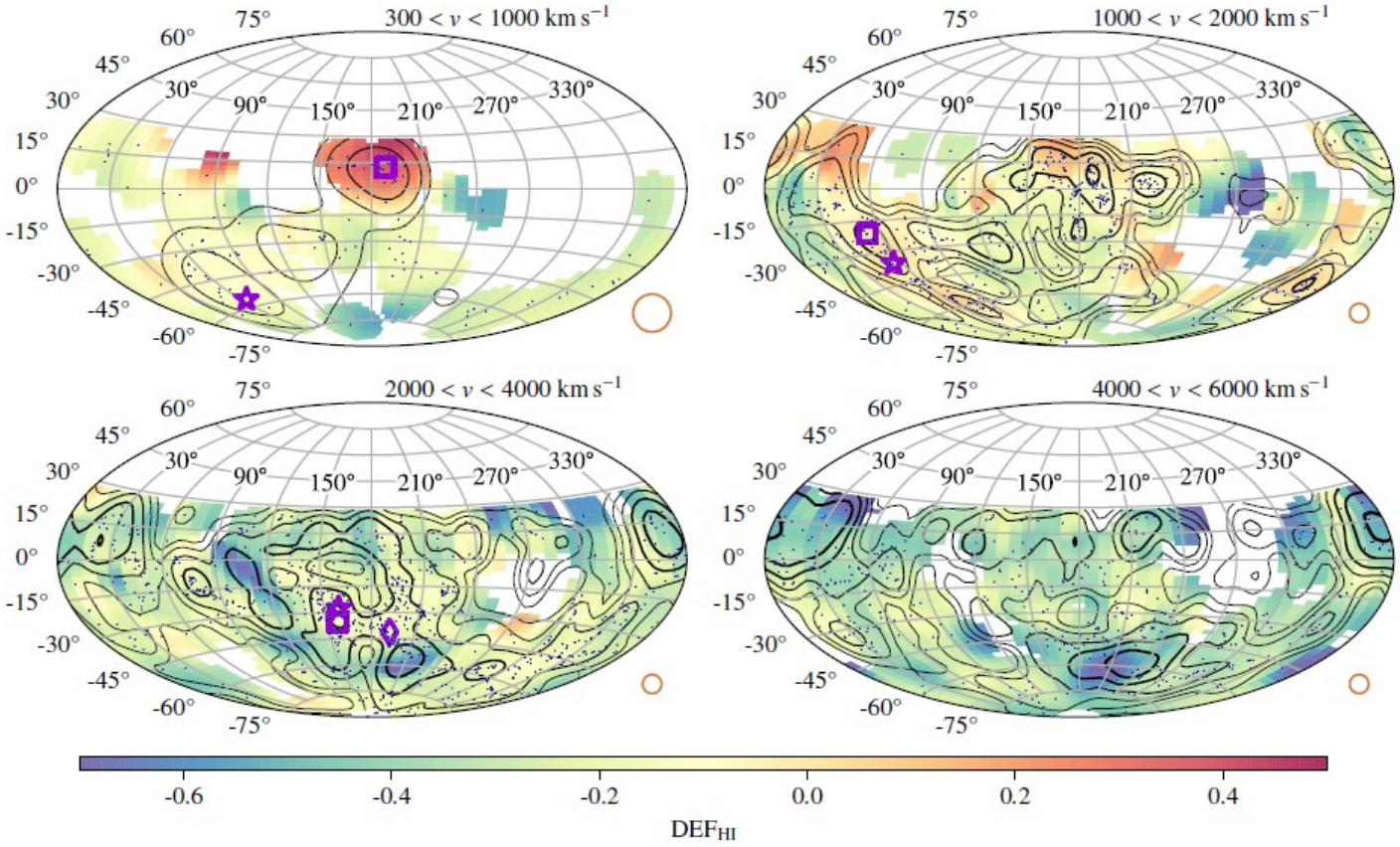

Figure 2. Gaussian weighted mean H I deficiency, DEF_{HI}, sky distribution plots. The Gaussian weighted mean DEF_{HI} increases from low (blue) to high (red) values, with white indicating there is no data. The contour levels indicate the underlying galaxy density distribution from HyperLEDA of $\log(N/\mathrm{sr}) = 1.9$, 2.2, 2.5, 2.8, 3.1, 3.4, 3.7 for increasing line thickness. The points indicate the location of HIPASS galaxies. The orange circles in the lower right corner of each panel indicates the size of the Gaussian (σ) kernel used to smooth each map as it appears at the equator. The four panels show the velocity ranges: V_1 = 300–1 000 km s^{-1}, V_2 = 1 000–2 000 km s^{-1}, V_3 = 2 000–4 000 km s^{-1} and V_4 = 4 000–6 000 km s^{-1} (top left, top right, bottom left and bottom right, respectively). The purple symbols indicate the positions of the Virgo cluster and Dorado group (square and star in top left panel, respectively), the Eridanus group and Fornax cluster (square and star in top right panel, respectively) and the Antlia, Hydra and Centaurus cluster regions (square, star and diamond in bottom left panel, respectively).

4 интервала скоростей

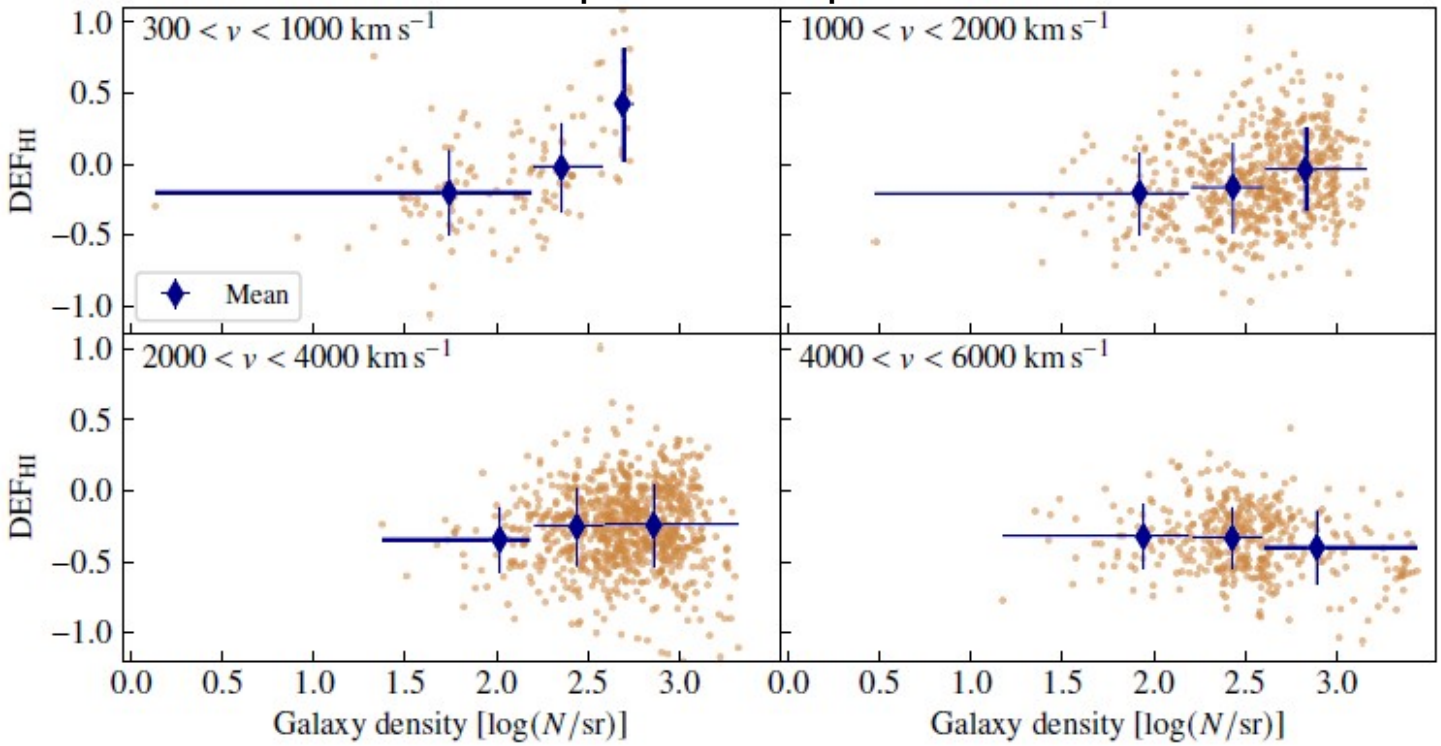

Figure 3. HIPASS galaxy H I deficiency, DEF_{HI}, vs projected surface density from HyperLEDA in the four velocity subsamples: V_1, V_2, V_3 and V_4 (top left, top right, bottom left and bottom right, respectively). The blue diamonds indicate the mean density and H I deficiency in each bin with vertical error bars showing the standard deviation (smaller than the mean symbols) and horizontal error bars showing the density range of galaxies in the bin.

омимо области VIRGO, корреляции отсутствуют

Асимметрия профилей

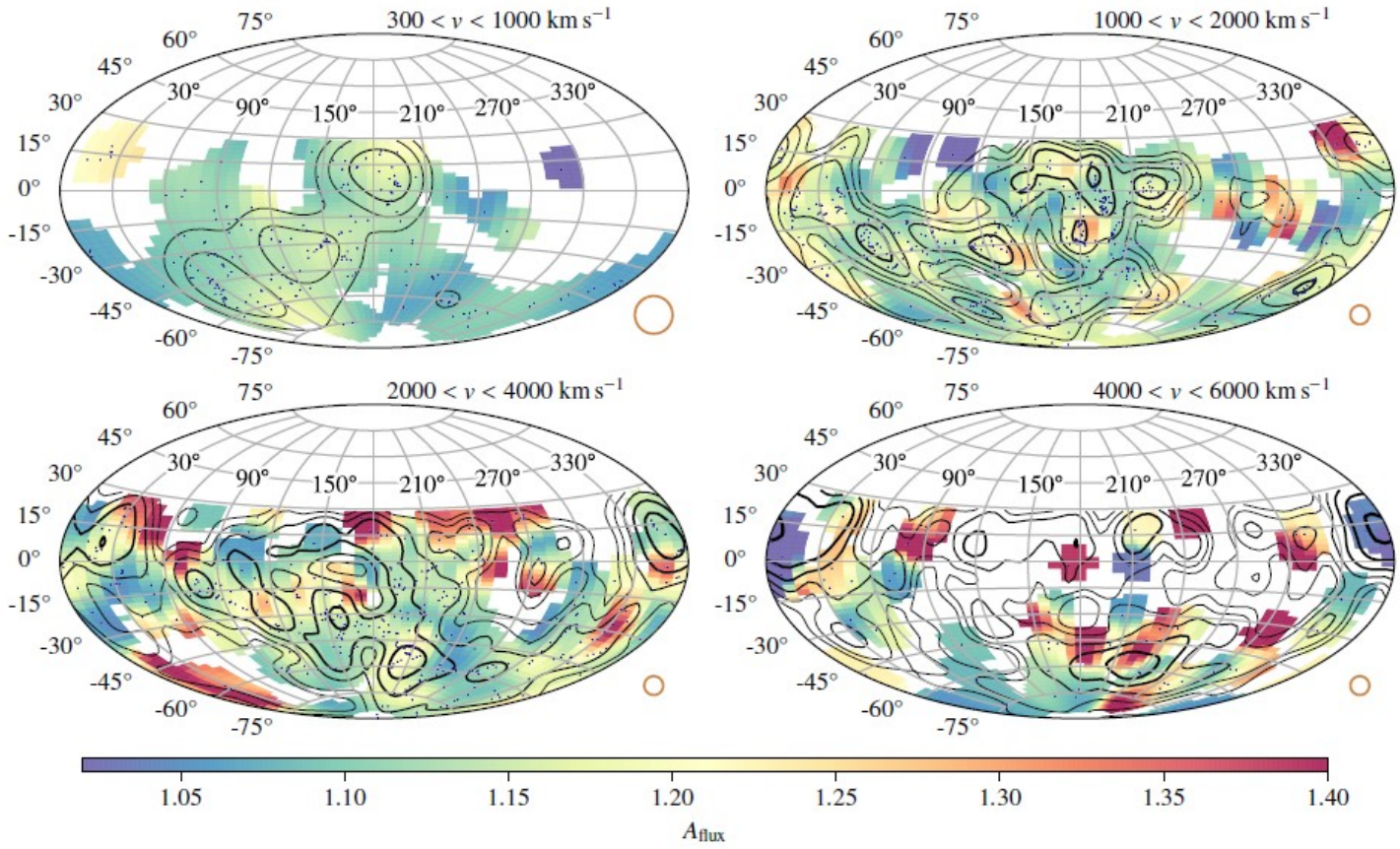

Figure 4. Similar plot to Figure 2 but for the Gaussian weighted mean flux ratio asymmetry, $A_{\rm flux}$. The contour levels indicate the underlying galaxy density distribution from HyperLEDA of $\log(N/{\rm sr}) = 1.9, 2.2, 2.5, 2.8, 3.1, 3.4, 3.7$ for increasing line thickness. Note that the HIPASS galaxy subsamples do not correspond to those in Figure 2 due to the different selection criteria (e.g. SNR > 30 for $A_{\rm flux}$ and selection criteria from Dénes et al. 2014 for $\rm DEF_{HI}$, Section 3.1).

Нет заметной корреляции асимметрии профиля с плотностями окружения

4 интервала скоростей

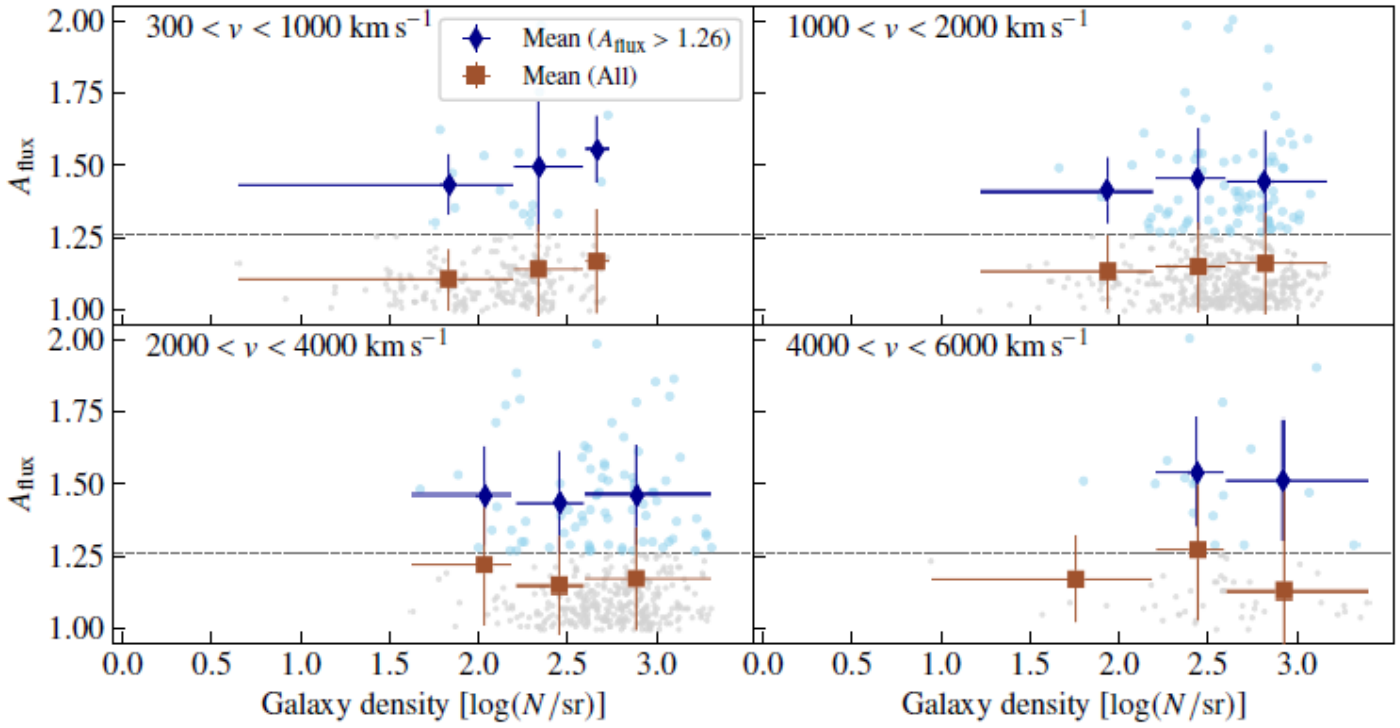

Figure 5. HIPASS flux ratio asymmetries, $A_{\rm flux}$, vs galaxy density. The grey and blue points are the values for individual HIPASS galaxies with $A_{\rm flux} < 1.26$ and > 1.26, respectively (i.e. cut at the Espada et al., 2011 2σ level, indicated by horizontal dashed line). The orange squares and blue diamonds indicate the mean density and $A_{\rm flux}$ for all galaxies and galaxies with $A_{\rm flux} > 1.26$, respectively, in each bin with vertical error bars showing the standard deviation and horizontal error bars showing the density range of galaxies in the bin.

Нет корреляций!

Связь асимметрии профилей с def HI

- Нет корреляци

Table 6. The fraction and mean and standard deviation of the flux ratio asymmetry, A_{flux}, for galaxies with $A_{flux} > 1.26$ and mean and standard deviation for all galaxies binned by H I deficiency, DEF_{HI}, from Figure 6.

DEF_{HI}	Fraction $A_{flux} > 1.26$	$\langle A_{flux} \rangle > 1.26$	$\langle A_{flux} \rangle$ All
−0.95	27% (7/26)	1.57 ± 0.27	1.25 ± 0.26
−0.51	13% (32/246)	1.47 ± 0.19	1.13 ± 0.20
−0.08	12% (38/314)	1.41 ± 0.15	1.13 ± 0.13
0.35	20% (12/61)	1.42 ± 0.14	1.16 ± 0.15
0.79	20% (1/5)	—	1.16 ± 0.23

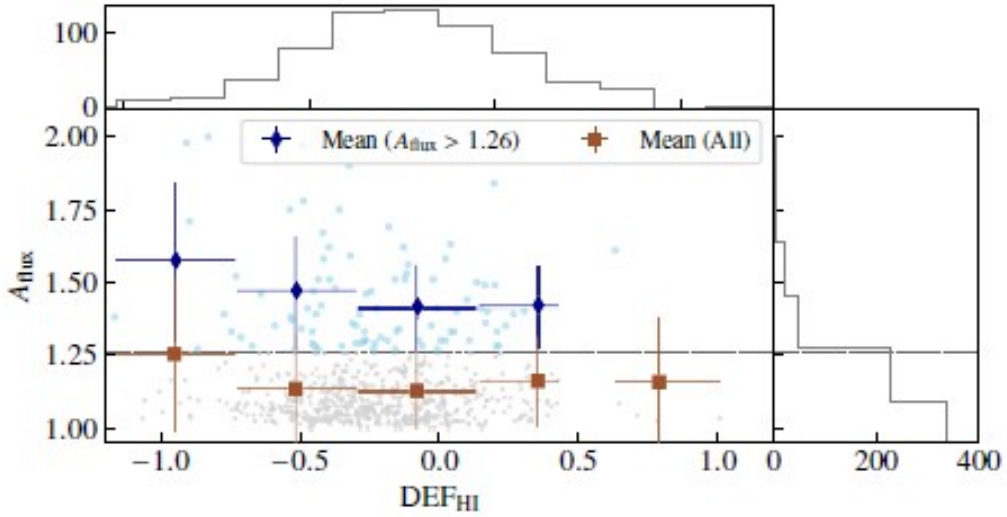

Основные выводы

- Помимо близких галактик, зависимость defHI – плотность не выявляется.
- Асимметрия профиля не зависит от плотностей на всех интервалах расстояний – кроме, возможно, галактик с аномально высоким содержанием HI

Resolving the Disc-Halo Degeneracy II: NGC 6946

S. Aniyan[1], A. A. Ponomareva[2,1,3⋆], K. C. Freeman[1†], M. Arnaboldi[4], O. E. Gerhard[5], L. Coccato[4], K. Kuijken[6] & M. Merrifield[7]

[1] *Research School of Astronomy & Astrophysics, Australian National University, Canberra, ACT 2611, Australia*
[2] *Oxford Astrophysics, Denys Wilkinson Building, University of Oxford, Keble Rd, Oxford, OX1 3RH, UK*
[3] *Kapteyn Astronomical Institute, University of Groningen, Postbus 800, NL-9700 AV Groningen, The Netherlands*
[4] *European Southern Observatory, Karl-Schwarzschild-Strasse 2, D-85748 Garching, Germany*
[5] *Max-Planck-Institut für Extraterrestrische Physik, Giessenbachstrasse, 85741 Garching, Germany*
[6] *Leiden Observatory, Leiden University, Niels Bohrweg 2, NL-2333 CA Leiden, the Netherlands*
[7] *School of Physics and Astronomy, University of Nottingham, University Park, Nottingham, NG7 2RD, UK*

Accepted XXX. Received YYY; in original form ZZZ

ABSTRACT

The mass-to-light ratio (M/L) is a key parameter in decomposing galactic rotation curves into contributions from the baryonic components and the dark halo of a galaxy. One direct observational method to determine the disc M/L is by calculating the surface mass density of the disc from the stellar vertical velocity dispersion and the scale height of the disc. Usually, the scale height is obtained from near-IR studies of edge-on galaxies and pertains to the older, kinematically hotter stars in the disc, while the vertical velocity dispersion of stars is measured in the optical band and refers to stars of all ages (up to $\sim$ 10 Gyr) and velocity dispersions. This mismatch between the scale height and the velocity dispersion can lead to underestimates of the disc surface density and a misleading conclusion of the sub-maximality of galaxy discs. In this paper we present the study of the stellar velocity dispersion of the disc galaxy NGC 6946 using integrated star light and individual planetary nebulae as dynamical tracers. We demonstrate the presence of two kinematically distinct populations of tracers which contribute to the total stellar velocity dispersion. Thus, we are able to use the dispersion and the scale height of the same dynamical population to derive the surface mass density of the disc over a radial extent. We find the disc of NGC 6946 to be closer to maximal with the baryonic component contributing most of the radial gravitational field in the inner parts of the galaxy ($V_{max}(\mathrm{bar}) = 0.76(\pm0.14)V_{max}$).

- Ключевой параметр при моделировании кривой вращения – это радиальное распределение массы диска. Обычно оно определяется через отношение M/L звездного населения.
- Стандартный подход:
- $\Sigma = f \cdot \sigma_z^2/Gh_z$
- Проблема в том, что оценки толщины диска и дисперсии скоростей относятся к разным звездным населениям. Толщина h_z – в red or NIR, а σ_z - в опт. диапазонах, т.е. для кинематически более холодного населения.

$$\Sigma_T = \Sigma_D + \Sigma_{C,*} + \Sigma_{C,gas} = \sigma_z^2/(2\pi G h_z),$$

- When attempting to break the disc-halo degeneracy by measuring the surface mass density of the disc, using the velocity dispersion and the estimated scale height of the disc, it is crucial that the dispersion and the scale height pertain to the same population of stars. The scale height, obtained from NIR studies of edge-on galaxies is for the older population of thin disc stars.

- Наблюдения:
- Анализ дисперсии скоростей звезд - VIRUS-W is an IFU spectrograph on the 2.7-m telescope at McDonald Observatory.
- Анализ дисперсии скоростей на больших расстояниях – по планетарным туманностям.
- Hershel telescope 4.2 м. Бесщелевой двух-дисперсный спектрограф + Hα - image.
- Отличие от HII: разграничение по яркости в [OIII].
- Ошибка измерения скорости PN – менее 9 км/с.

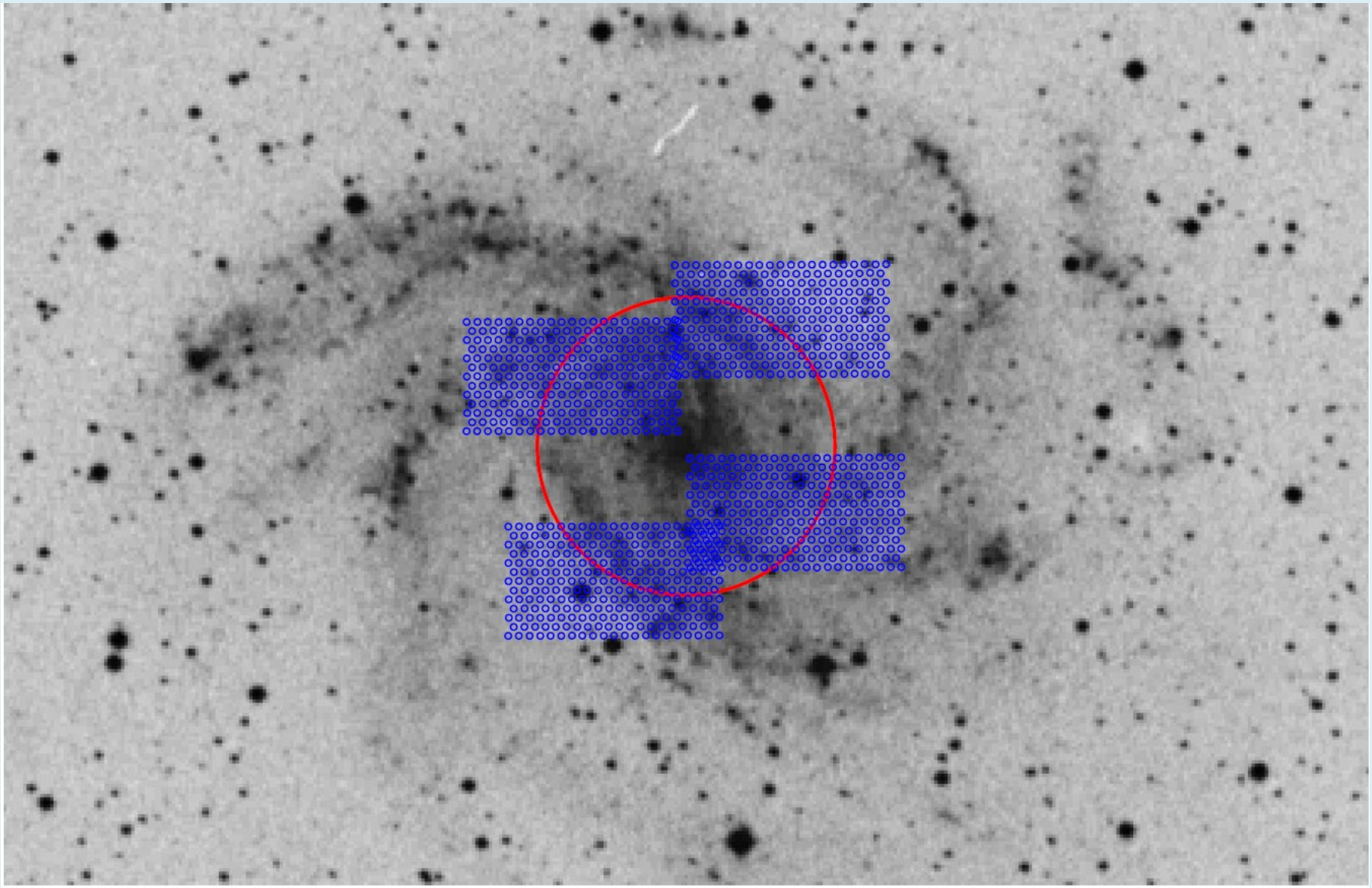

Figure 1. The positions of the four VIRUS-W IFU fields showing the 267 fibres in each field overlaid on a DSS image of NGC 6946. The red circle at a radius of 75″ shows the separation between our inner and outer radial bins.

4 поля. Разбиение на внутреннюю и внешнюю

Douglas et al 2002

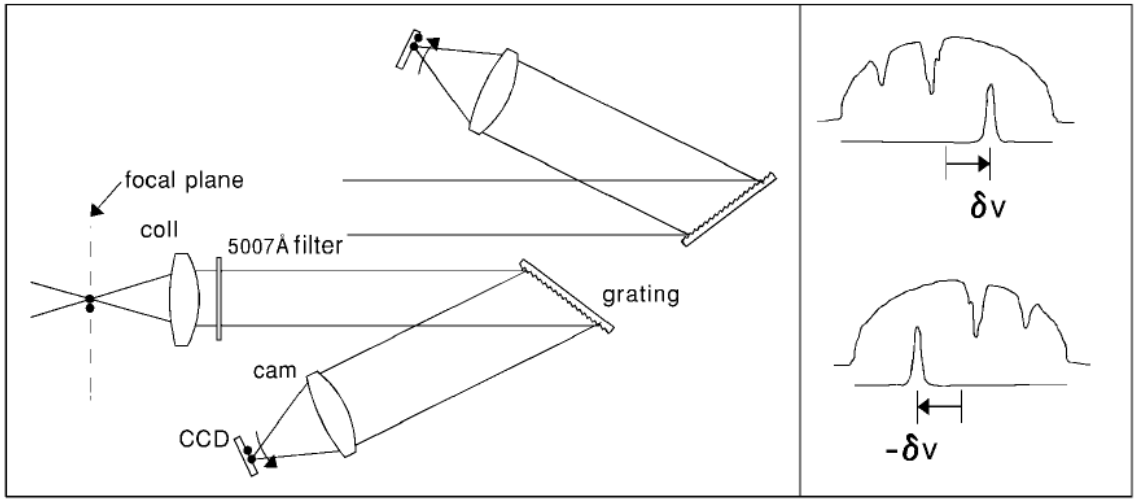

FIG. 2.—*Left:* Illustration of counterdispersed imaging; the arrow denotes the dispersion direction. *Right:* Corresponding images of a star and planetary nebula shown sc

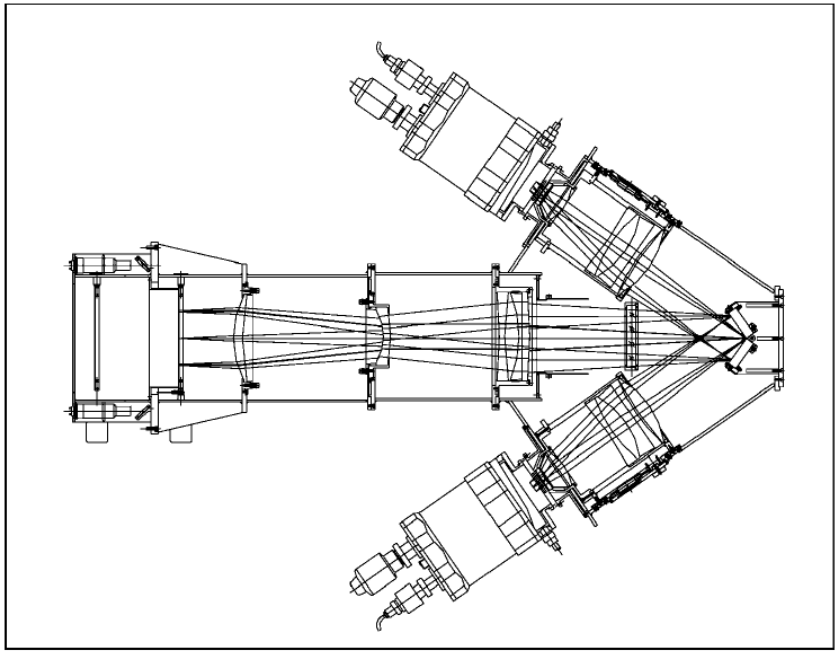

FIG. 4.—PN.S schematic. The pupil-splitting dual-grating mount is at the right of the figure, with the interference filter just to the left. The camera optics appear

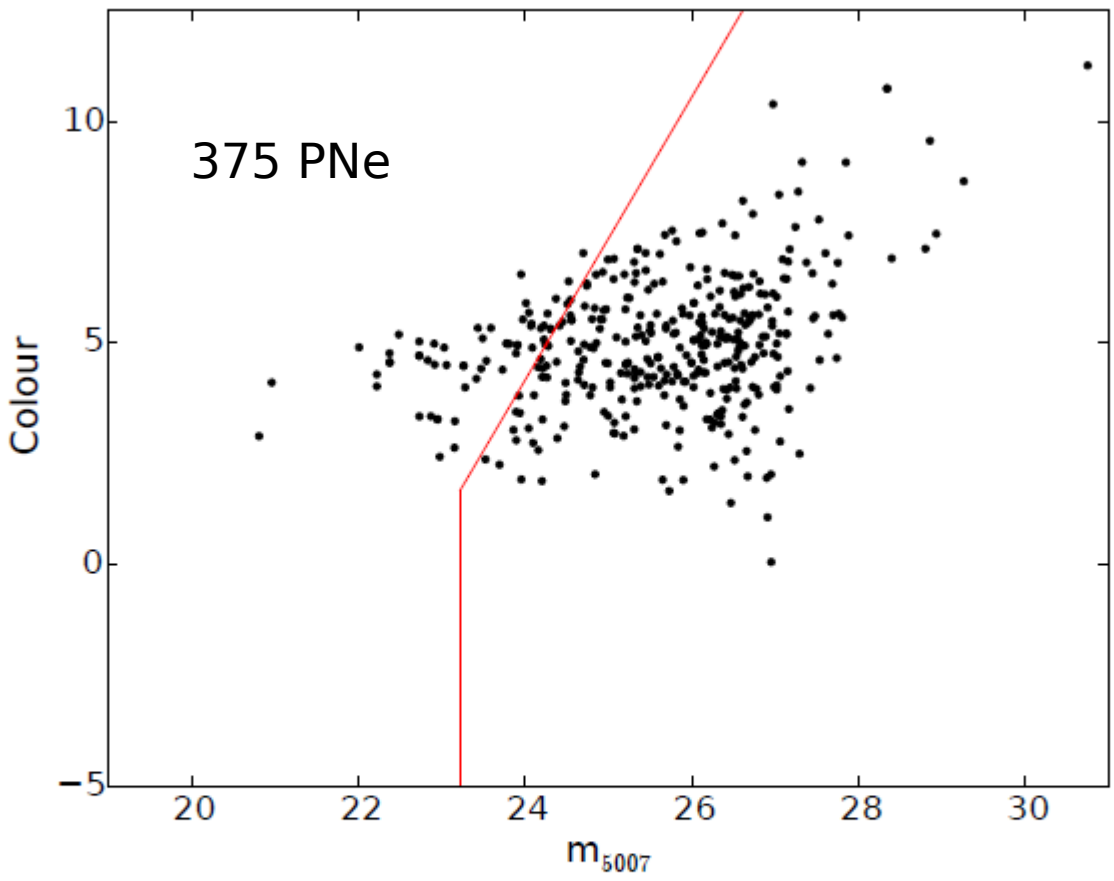

Figure 3. The colour-magnitude plot for [OIII] sources in NGC 6946. The vertical axis is the ([OIII] - Hα) colour and the horizontal axis is the m_{5007} magnitude. The PNe lie to the right of the red lines. Only these objects are used in our analysis.

Области покрыти

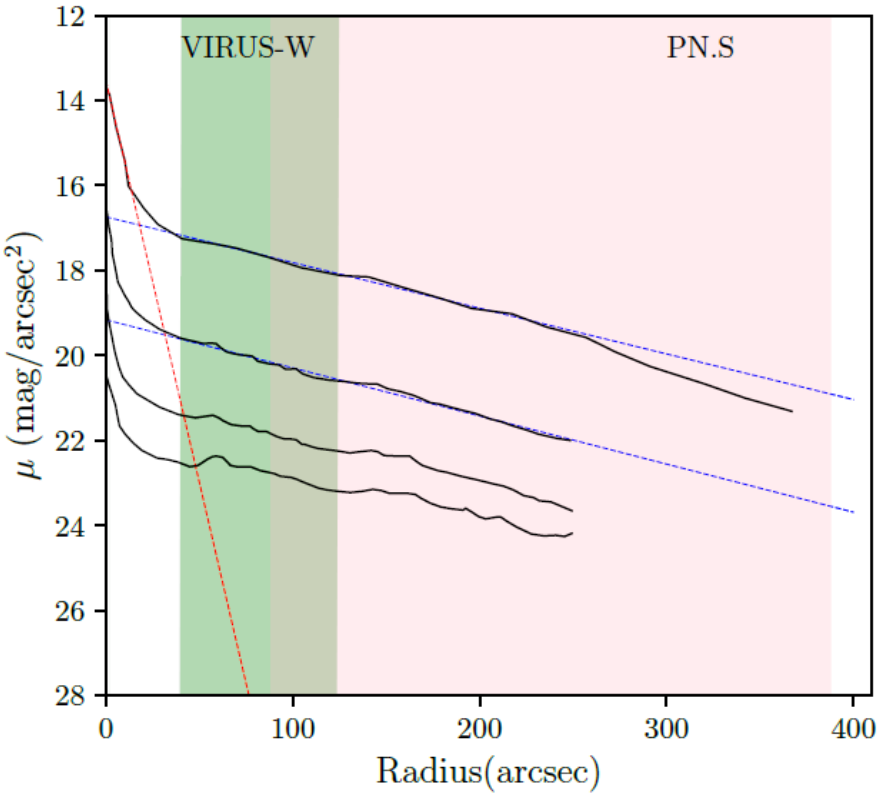

Figure 4. The surface brightness profiles of NGC 6946 in BVI (Makarova 1999) and 3.6 μm band (Muñoz-Mateos et al. 2009) are shown from bottom to top. The surface brightness is shown in VEGA magnitudes. The contribution to the light from the stellar disc in I-band is shown with blue line. The contributions to the total light from bulge and disc in the 3.6 μm band are shown with red and blue lines respectively. The average error on the surface brightness is ∼0.01 mag for the 3.6 μm band and ∼0.02 mag in the optical bands. The radial extent of the Virus-W and PNS data is shown with green and pink bands respectively.

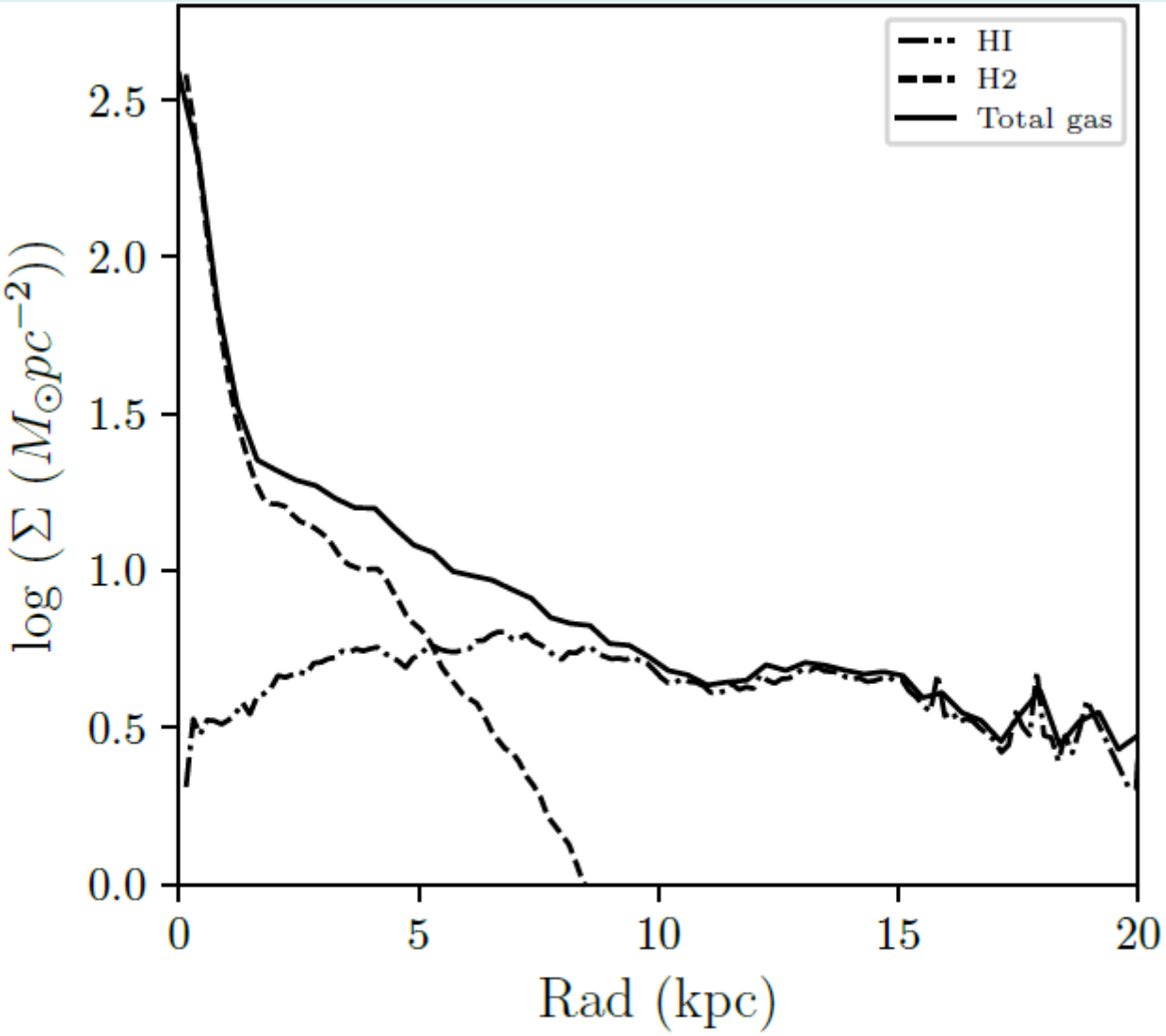

Figure 5. Surface mass density of the cold gas (atomic and molecular) in NGC 6946. The HI density profile derived from THINGS data (Walter et al. 2008) is shown with the dot dashed line. H2 profile derived from the HERACLES data (Leroy et al. 2009) is

- Обработка. 2-компонентный диск. Моделирование с использованием template stellar spectra.

Mean Radius (arcsec)	2 component Model			1 Component Model	
	$\sigma_{z,cold}$ (km s^{-1})	$\sigma_{z,hot}$ (km s^{-1})	BIC	σ_z (km s^{-1})	BIC
144	$\leq 12.1 \pm 2.3$	32.0 ± 6.4	1236	26.5 ± 1.7	1251
242	$\leq 12.9 \pm 3.3$	20.9 ± 4.1	1076	18.6 ± 1.2	1090
335	$\leq 12.3 \pm 3.5$	14.8 ± 5.9	1062	14.5 ± 1.0	1055

Table 4. The σ_z values calculated from the PN.S data. We give the 90% confidence upper limit for the cold dispersions. The lower BIC values of the two component fit suggest it to be the preferred model over the one component model, except for the outermost radial bin where the one component model is preferred.

$$\sigma^2_{LOS} = \sigma^2_\theta \cos^2\theta . \sin^2 i + \sigma^2_R \sin^2\theta . \sin^2 i + \sigma^2_z \cos^2 i + \sigma^2_{meas} \quad (3)$$

where σ_R, σ_θ and σ_z are the three components of the dispersion in the radial, azimuthal and vertical direction, σ_{meas} is the measurement error on the velocity and i is the inclination of the galaxy ($i = 0$ is face-on). Using the epicyclic approximation in the part of the rotation curve that is close to solid body, we adopt $\sigma_R = \sigma_\theta$, and for the part of the rotation curve that is flat, we adopt $\sigma_R = \sqrt{2}\sigma_\theta$.

We also adopt the stellar velocity ellipsoid parameter z=R ratio to be 0.6 $\pm$0.15 following the result from Shapiro et al.

- Толщина слоя считается фиксированной (для старых звезд). Оценка h_z - через scaling relation

Bershady et al. (2010):

$\log(h_R/h_z) = 0.367 \log(h_R/\mathrm{kpc}) + 0.708 \pm 0.095$

Взято $h_R = 2.8$ kpc из фотометрии.

- Наблюдаемая дисперсия скоростей:
- Звездные линии поглощения в области VIRUS-W и PNe – во внешней области.
- Привязка к скоростям – по HI velocity field по THINGS с учетом асимметричного дрейфа для звезд..

Сравнение спектров холодного и теплого звездного

- Холодный

компонент молох

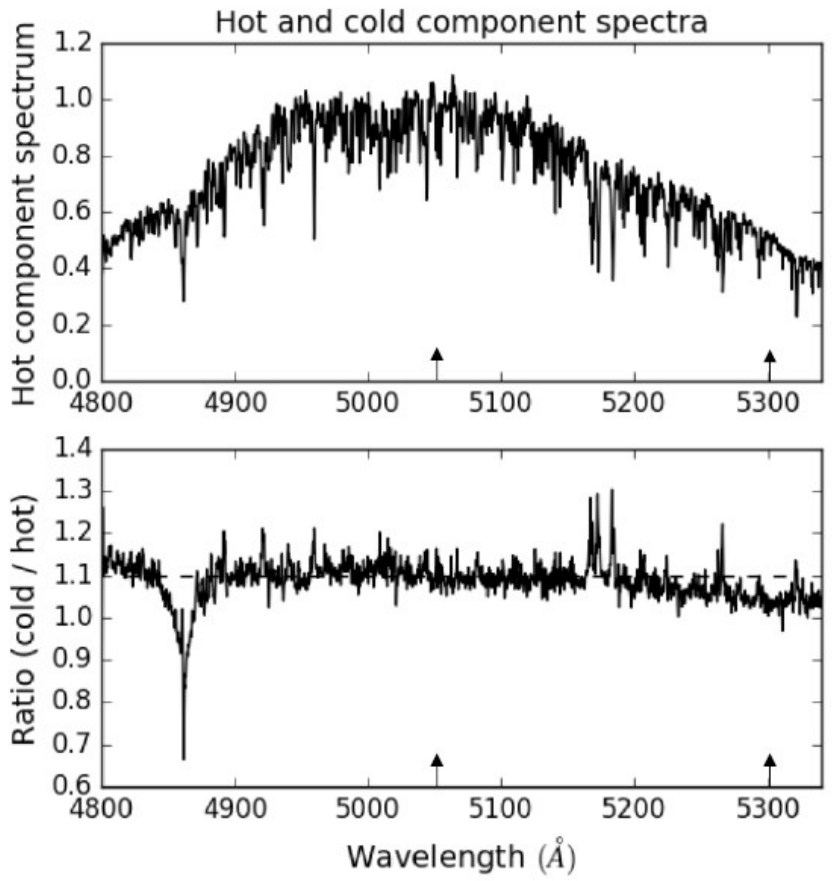

Figure 11. The upper panel shows the spectrum for the hot component for the inner radial zone in NGC 6946. The lower panel shows the ratio of the cold to the hot spectra, pixel by pixel. The spectral region between 5050 and 5300 Å used for the fit is indicated with vertical arrows. The [NI] emission lines at ∼ 5200 Å have been omitted from the fit.

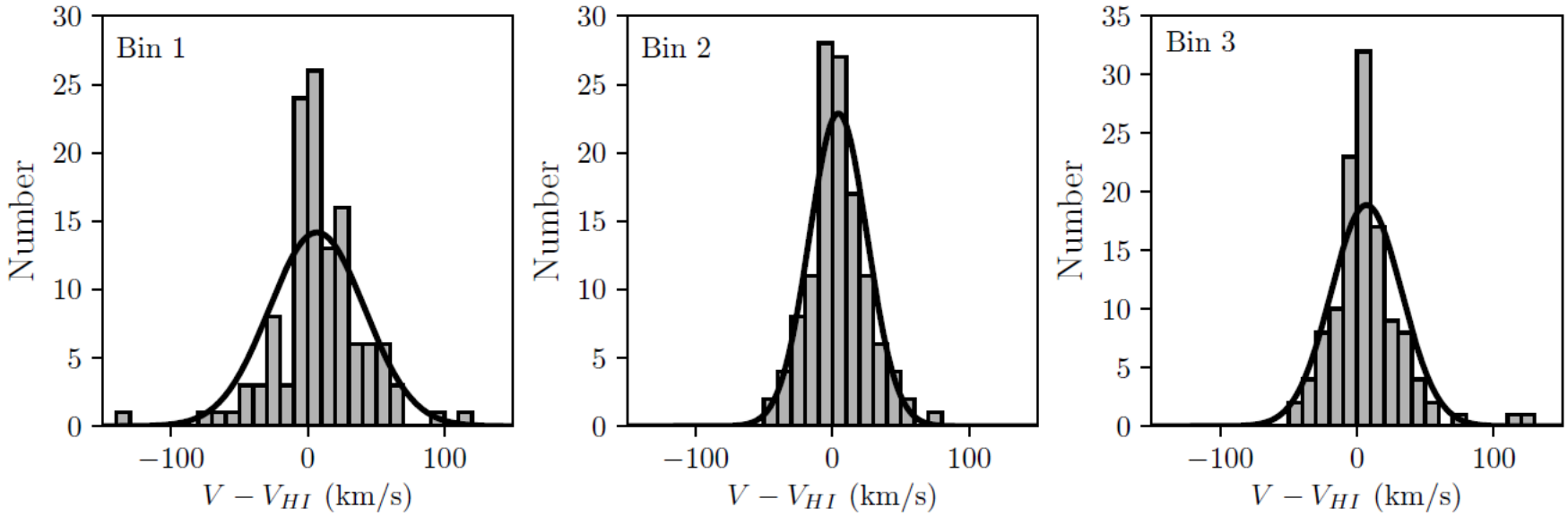

Figure 9. The distribution of the PNe line-of-sight velocities from the bottom panels in Figure 8 for each radial bin respectively. The single Gaussian fit to the data is shown with the black curve. The velocity distributions are not well represented by a single Gaussian: the excess of low-velocity PNe is evident.

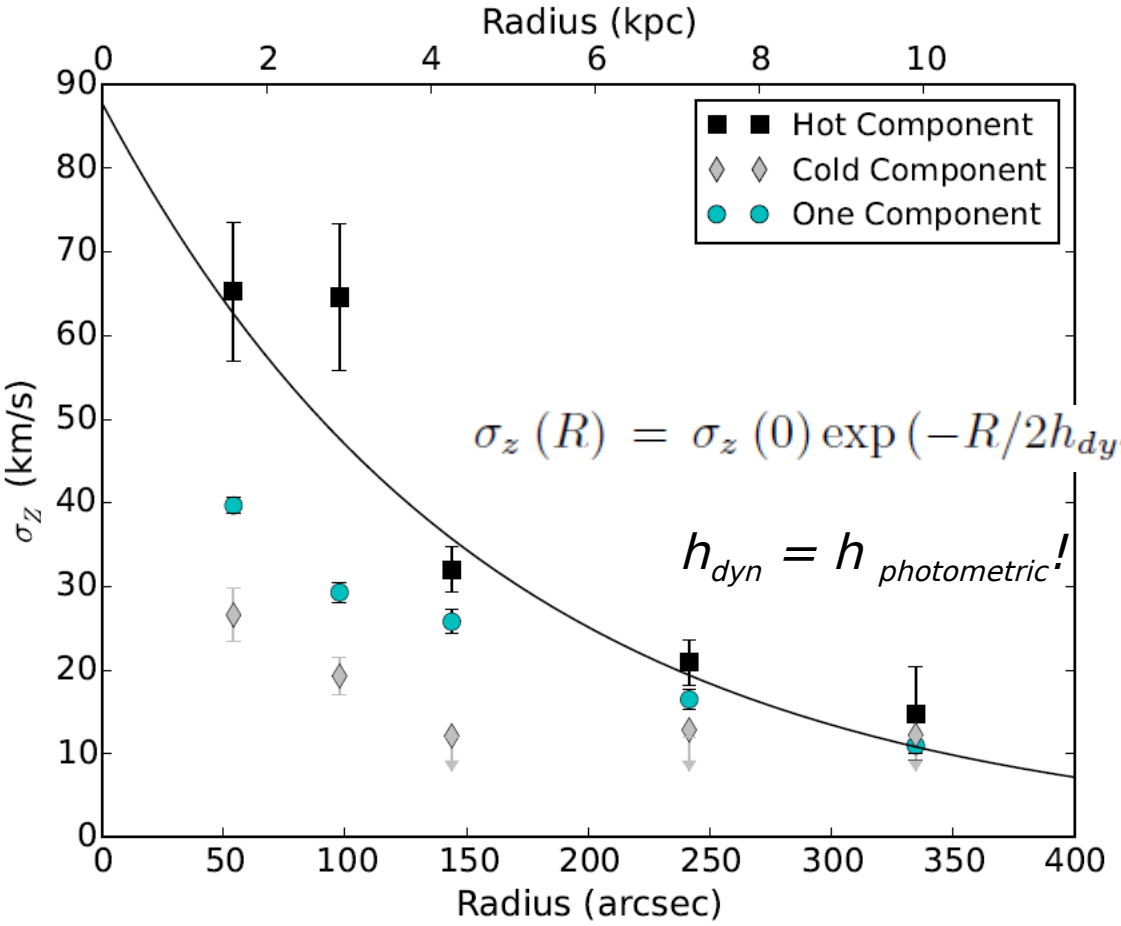

Figure 10. The vertical velocity dispersion as a function of radius in NGC 6946. The black and grey markers indicate the hot and cold velocity dispersions respectively from our two component fits, the cyan markers are our single-component values. The two inner data points at $R = 54''$ and $98''$ were obtained for integrated light spectra from VIRUS-W and the outer data points are for PNe from PN.S. The solid line denotes an exponential with twice the galaxy's dynamical scale length ($h_{dyn} = 92'' = 2.72$ kpc) fit to the hot component. Our data have been corrected for the HI velocity dispersion and PNe measuring errors. The cold component from the PN.S data were dominated by our errors, and we show the 90% upper limits for these values. The errors bars are the 1σ errors obtained from Monte Carlo simulations.

Кривая вращения взята по THINGS

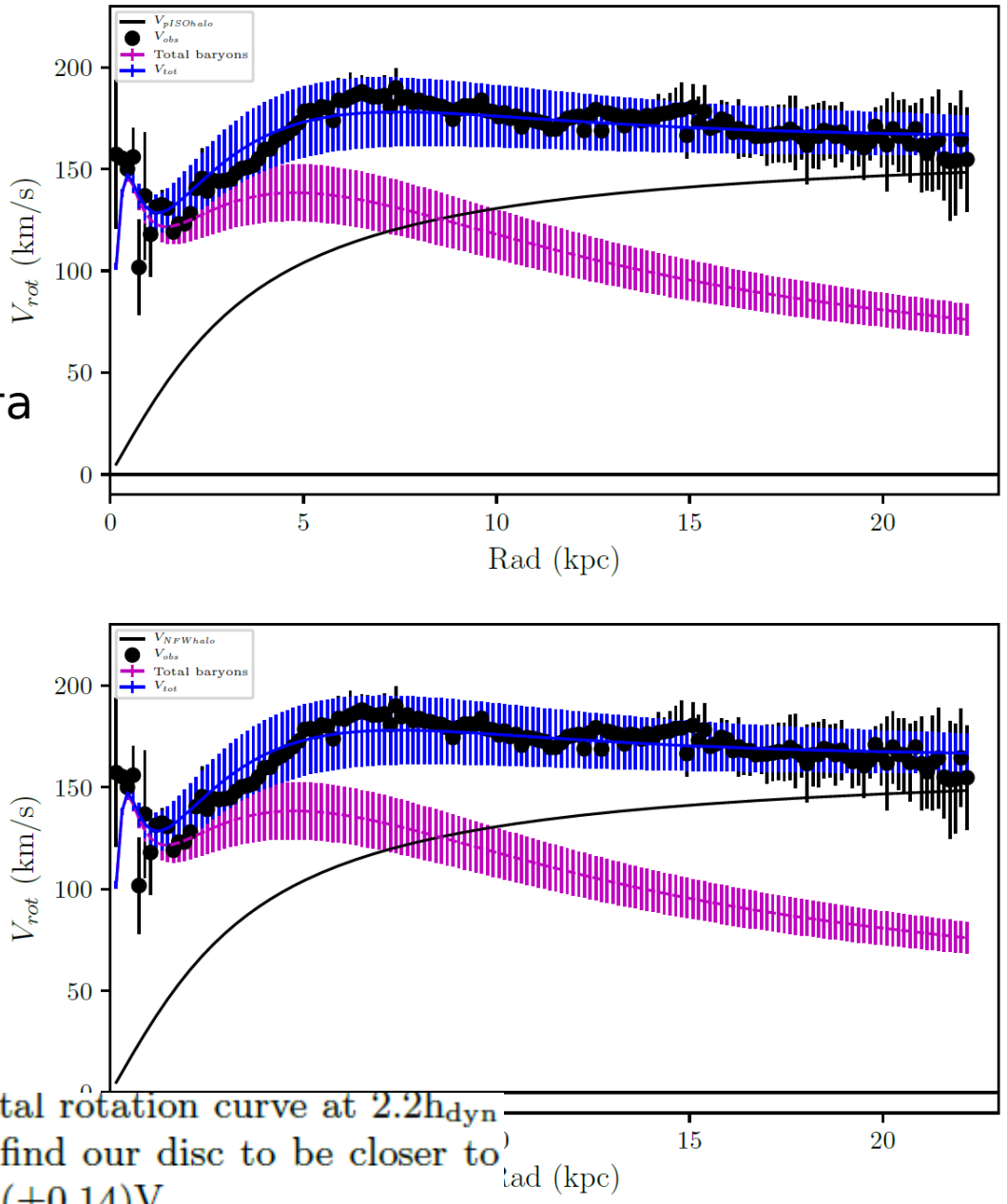

From the maximum velocity of the total rotation curve at $2.2h_{dyn}$ ($V_{max} = 170 \pm 10$ km s^{-1}) we find our disc to be closer to maximal with $V_{max}(bar) = 0.76(\pm 0.14)V_{max}$.

Figure 13. The rotation curve decomposition for NGC 6946 by fitting a pISO halo (top panel) and a NFW halo (bottom panel). The observed HI rotation curve is shown as black dots. The magenta dashed line is the rotation curve from the total baryonic component: bulge+gas+disc with the 1σ errors. The blue line represents the total rotational velocity: $V_{tot}^2 = V_{bar}^2 + V_{halo}^2$. The short blue vertical lines show the 1σ errors of the modelled total rotational velocity. 1kpc = 33.8″.

Основные выводы

- We show that there exists a younger, kinematically colder population of tracers within an older and hotter component.

- Оценка плотности диска получилась в 2-3 раза выше, чем без учета двух компонент тонкого диска с разной дисперсией скоростей.
- Динамическая шкала диска по профилю дисперсии скоростей совпала с фотометрической на 3.6 мкм – в пользу постоянной толщины диска. След., M/L почти не меняется с радиусом.
- Среднее отношение $M/L_{3.6}$ = 0.4 получается ниже, чем для имеющихся звездных моделей (0.6): вклад пыли и AGB stars?
- Модель согласуется с maximum disc – как и ранее полученная для NGC628.
- The baryons together dominate the radial component of the gravitational field out to a radius of about 8 kpc.